Tellus (1994), 46A, 635–650
Printed in Belgium – all rights reserved

TELLUS
ISSN 0280–6495

Numerical simulation of the northern Germany storm of 27–28 August 1989

By SIGBJØRN GRØNÅS, NILS GUNNAR KVAMSTØ and ELMER RAUSTEIN*, *Geophysical Institute, University of Bergen, Allegaten 70, 5007 Bergen, Norway*

(Manuscript received 10 September 1992; in final form 6 October 1993)

ABSTRACT

On 27 August 1989, an unusual mesoscale storm struck the area between Hamburg and Kiel in Germany. Locally, more than 100 mm of precipitation fell in 24 h, and mean winds exceeding 25 m s^{-1} were recorded. The operational models failed to predict both the development of the originally innocent-looking low, and its track. Successful simulations have been performed for this situation by introducing the Sundqvist scheme for parameterization of the hydrological cycle into the Norwegian operational limited area model. The simulations show that latent heat release is the main driving mechanism in the intensification of the low. Comparison between simulations with and without released latent heat taken into account shows significant differences in the development and also in track, and clearly demonstrates the role of released latent heat in generation and clustering of the *PV*, and its subsequent importance for spinning up the mesoscale vortex.

1. Introduction

A severe mesoscale storm hit the Schleswig-Holstein area in Northern Germany from noon 27 August 1989 until the next morning (see Figure 1b for geographical names). More than 100 mm of precipitation during 24 hours were measured over the Kiel and Hamburg area (about 100 × 100 km), and wind gusts of more than 30 m s^{-1} at the Baltic coast close to Kiel. As described by traditional synoptic surface weather maps the phenomenon might be characterized as a strengthening of the pressure gradient in the cold air of a weak low with a pronounced low-level warm temperature wave. This strengthening caused the low to follow a different track than was predicted. The storm was not at all captured by the operational numerical models and was not forecasted by the German weather service.

It has earlier been demonstrated, e.g., by Kristjansson (1990), that similar mesoscale weather systems might be predicted with state-of-the-art high resolution numerical models (horizontal grid length of 50 km or less). In this paper the Norwegian limited area operational model has been used for simulations of the storm in order to investigate its mesoscale predictability and dynamical/thermodynamical origin. A short description of the model and the set-up of our experiments are given in section two.

The synoptic scale development takes place over land near the coast in an area with a relatively dense network of radiosonde stations, and high quality analyses might be expected. A short description of the synoptic evolution of the storm is given in section three. The evolution of the model storm in the best simulation is described in section four together with verification of the storm track, precipitation and surface wind.

How can this unusual development be explained? What causes the development? Why did the low follow a different track than predicted? Such dynamical aspects are discussed in section five on the basis of potential vorticity thinking according to Hoskins et al. (1985) (HMR in the following), a concept which has been used by several authors to explain cyclogenesis of extratropical cyclones (e.g., Davis and Emanuel, 1991).

* Corresponding author.

2. The numerical model

The numerical model used is the Norwegian high resolution limited area numerical model, here called NOLAM, developed by the Norwegian Meteorological Institute (see Grønås and Hellevik, 1982; Grønås et al., 1987; Nordeng, 1986). The σ coordinate primitive equations are integrated on a stereographic map with u, v, θ, q and p_s as dependent variables.

The explicit time-integration method used is based on the time-staggered F-scheme proposed by Eliassen (1956) and modified by Bratseth (1983). In addition, the Schuman pressure averaging technique is applied as done by Brown and Campana (1978). The initialization is according to Bratseth (1982, 1987, 1989). The intermittent data assimilation system providing the analysis used for this study is described by Grønås and Midtbø (1987). The analysis method is based on a multivariate successive correction scheme proposed by Bratseth (1987). Humidity is analyzed with an univariate scheme using radiosonde observations only.

The physical parametrization in NOLAM is made by Nordeng (1986). The surface fluxes are according to Louis et al. (1981) with exchange coefficients from Blackadar (1979). Convection corresponds to Geleyn (1985). Clouds are derived diagnostically from relative humidity. A more sophisticated treatment of condensation and clouds was introduced by Sundqvist et al. (1989), and this treatment was introduced in the latest version of NOLAM by Kvamstø (1992). This model version is here called UBLAM.

In the Sundqvist condensation and cloud scheme the cloud water is a prognostic variable through a continuity equation for this variable. The stratiform cloud scheme is identical to the one described by Manabe et al. (1965), except for the inclusion of cloud water. The convective condensation uses the Kuo scheme (Kuo, 1965, 1974), but modified to include cloud water as a prognostic variable.

In 1990, the operational NOLAM was extended to the stereographic integration area in Fig. 1a with a grid distance of 50 km at 60° North (121×97 grid points) and 18 levels in σ-coordinates below 100 hPa (Grønås, 1990). In Fig. 1a is also shown the positioning of the σ-levels when p_s is 1000 hPa. The operational integration area and resolution have been used in our experiments.

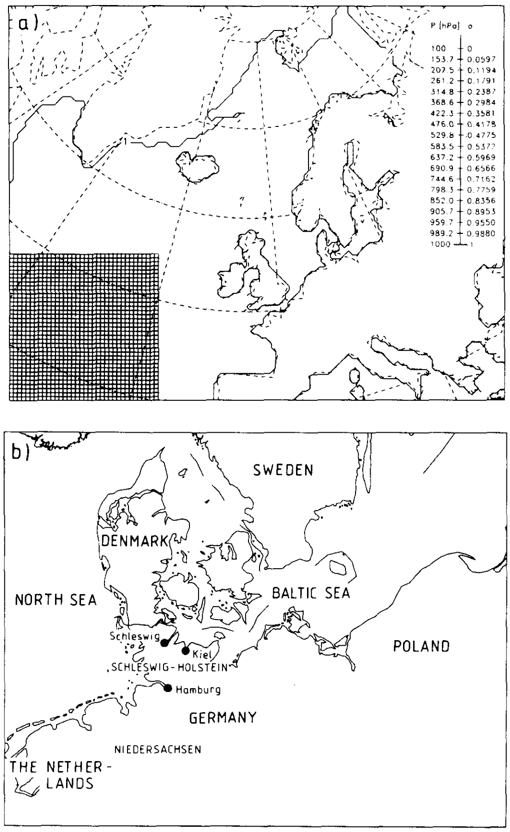

Fig. 1. (a) The integration area on a polar stereographic map projection true at 60° N. The solid line is the land-sea mask. The grid in the lower left corner indicates the horizontal grid resolution. On the right, the vertical distribution of the 19 σ-levels together with the corresponding pressure values with a surface pressure of 1000 hPa is shown. (b) Map with geographical names referred to in the text.

The initial conditions and lateral boundary values have been prepared from pressure analyses of u- and v-components of the wind, geopotential and relative humidity at 11 standard pressure levels between 100 and 1000 hPa including 925 hPa. These analyses from DNMI have been available on a stereographic grid with 150 km grid distance at 60° North. All analyses have been interpolated to the σ-levels of the model by linear interpolation in the Exner function. The lateral boundary values are incorporated every 6 hours. Since cloud water is not included in the assimilation scheme of NOLAM, all experiments start out with zero cloud water everywhere and at lateral boundaries the cloud water is zero at all times. The surface parameters are those of operational NOLAM except that here climatological sea surface temperature (SST) has been used.

The UBLAM gave significant better simulation of the storm than NOLAM. Since the main purpose of the investigation is to get a good simulation and to understand its dynamics, we pay little attention to the differences in the simulations of UBLAM and NOLAM. With UBLAM, two experiments will be discussed here:

- The standard run with the standard model with physical parametrization every time step.
- The dry run which is the same as the standard run except that latent heat is not released.

3. Observational analysis of the storm

A routine description of the storm has been given by H. Erdmann 29 August 1989 in the journal "Wetterkarte des Deutschen Wetterdienstes, Amtsblatt des Seewetteramtes und der Wetteramter Bremen, Essen, Hannover und Schleswig" edited by Deutscher Wetterdienst Seewetteramt, Hamburg. The surface wind and precipitation values used for verification have been taken from this publication, but checked afterwards by The German Weather Service, Offenbach. According to Erdmann a rather weak low was predicted to move eastward from England toward central Germany. The forecasters did not discover any signs of an unusual development of the low, so no exceptional wind or precipitation was expected.

At 00 UTC 27 August, there is a north-westerly jet from Iceland over Britain with maximum winds of more than $50 \mathrm{~m~s^{-1}}$ at 300 hPa. East of this jet there is a short wave in the height field (not shown). At 500 hPa this is seen as a cold, flat low, with the coldest air at the southern tip of Norway, and a ridge further north. The temperature range between the trough and the warm ridge is less than 5°C.

Figs. 2a, b show two surface weather maps from DNMI (Bergen Office) with mean sea level pressure (MSLP), frontal positions and precipitation areas. The maps agree very well with German weather maps. At 00 UTC 27 August the surface low was centred just outside the coast of the southern Netherlands (Fig. 2a). During the following 30 hours the centre of the low followed the track indicated in Fig. 2a. Figs. 2a, b show that there is hardly any deepening or filling of the low throughout the period. What is apparent, however, is a significant increase in the pressure gradient and wind to the west and north of the low, from the surface and up to at least 850 hPa (see also Fig. 6b). The track of the low makes a peculiar bend northward during approximately 12 h from late afternoon on 27 August. The low moved more than 100 km northward, returned the same distance and retained the easterly track.

The position of the surface fronts indicates an occluded frontal wave moving eastward. At 00

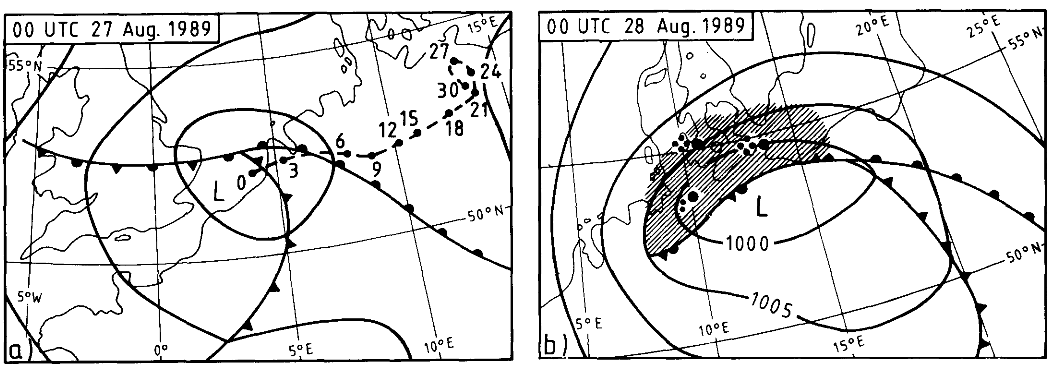

Fig. 2. (a) Surface analysis at 00 UTC 27 August 1989. The track of the low is plotted every 3 h. The numbers above (or below) the dots are hours from 00 UTC 27 August. (b) Surface analysis at 00 UTC 28 August 1989. Stations showing strong precipitation are plotted. The main precipitation area is hatched.

UTC 28 August the cold front has crossed most of Germany and the occlusion stretches from northern Poland towards Holstein at the Baltic coast, and further over Nieder-Sachsen. At this time many stations north and west of the occlusion reported continuous vigorous rain. The mean wind speeds were more than 20 m s^{-1} at the Baltic coast and at the sea area outside. The maximum gusts as given by the synoptic stations were reported to 33 m s^{-1}.

4. Verification

Fig. 3 shows MSLP after 24-h integration valid at 00 UTC 28 August and the modeled track of the surface low. First, the track of the model low compares very well with the actual one (Fig. 2a). The sudden and unexpected turning towards a northerly direction, followed by a movement in southerly direction some hours later, are almost perfectly predicted. The position of the model low is, however, shifted somewhat to the south compared with the observations. The near constant pressure in the centre of the low, and the increasing pressure gradient and thereby increasing wind west and north-west of the low are also in accordance with the subjective analyses. The strongest increase in geostrophic wind is found during the afternoon (see Table 1), and at midnight a value of 62 m s^{-1} is reached.

The synoptic surface wind observations correspond nicely to the wind in the lowest model σ-level (40 m) (see Fig. 4). The strongest wind

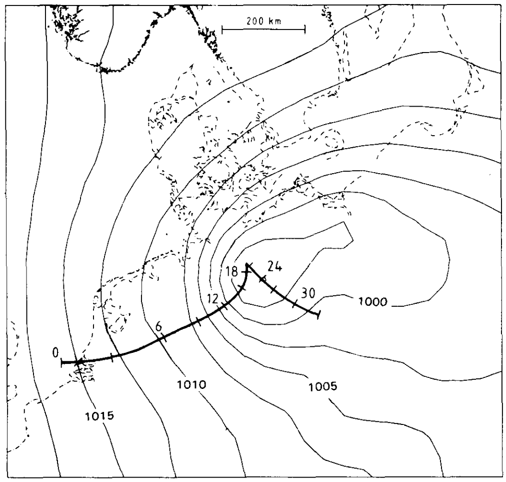

Fig. 3. 24-h simulation of mean sea level pressure (in hPa), valid at 00 UTC 28 August 1989. The heavy line shows the track of the low pressure centre, with tick marks every 3 h during the simulation.

(20 m s^{-1}) is found at midnight and three hours after midnight (see Table 1).

Fig. 5 shows that both quantitatively and with respect to distribution, the correspondence between observed and modeled precipitation (24-h accumulated values) is very satisfactory. The maximum predicted sums are close to 125 mm and observations at two stations show a little more than 100 mm. Again, the position in the model is shifted a little bit southward compared with the observations. Considering that the precipitation

Table 1. *Max surface geostrophic wind, max wind at 40 m height, max and min surface pressure tendency, max 3-hourly precipitation and minimum surface pressure in low (2 last digits); all from simulation. The last line gives the analyzed minimum surface pressure in low (2 last digits)*

Prog. time (h)	0	3	6	9	12	15	18	21	24	27	30
V_{gs} (max)(m/s)	17	18	20	28	35	40	48	54	62	60	53
$V_{40\,m}$ (max)(m/s)	13	13	13	13	13	13	15	17	20	20	17
$\left(\frac{\partial p_s}{\partial t}\right)_{max} \left(\frac{hPa}{3\,hr}\right)$		0	1	1	2	2	2	3	1	3	5
$\left(\frac{\partial p_s}{\partial t}\right)_{min} \left(\frac{hPa}{3\,hr}\right)$		−2	−2	−2	−2	−3	−2	−1	−1	−1	1
$p_{3\,h}$ (max)(mm)		1	5	11	22	25	25	25	25	24	22
$p_{sL(sim)}$ (hPa)	02	02	01	00	98	97	96	96	95	96	98
$p_{sL(ana)}$ (hPa)	02	99	99	99	98	97	97	98	97	98	99

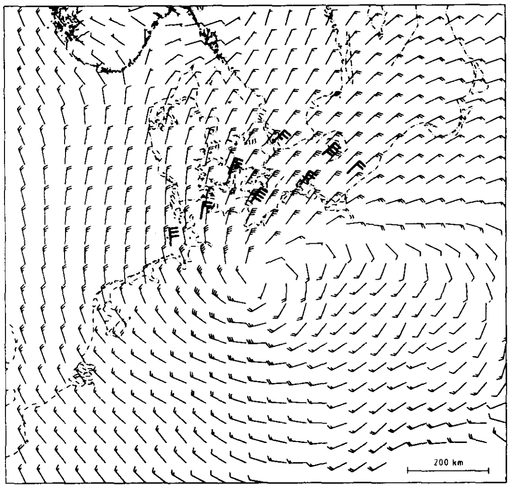

Fig. 4. 24-h simulation of wind in the lowest σ-layer, valid at 00 UTC 28 August 1989. The heavy arrows are observed surface winds. Long tag on the back of the arrow means 5 m/s, short tag means 2.5 m/s.

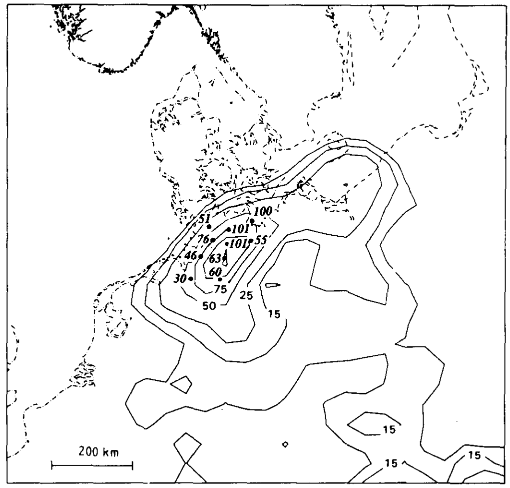

Fig. 5. Simulation of 24-h accumulated precipitation, valid at 06 UTC 28 August 1989. Observed 24-h accumulated precipitation is plotted for selected stations.

in many places was near record-high in this flat terrain, the agreement is remarkable. The maximum intensity of the predicted precipitation every third hour, as given by the accumulated value during three hours (see Table 1), shows, as for the wind, that the increase takes place during the afternoon and evening.

The observed and predicted sounding 00 UTC 28 August at station Schleswig (Fig. 6) both show a deep moist layer with low static stability.

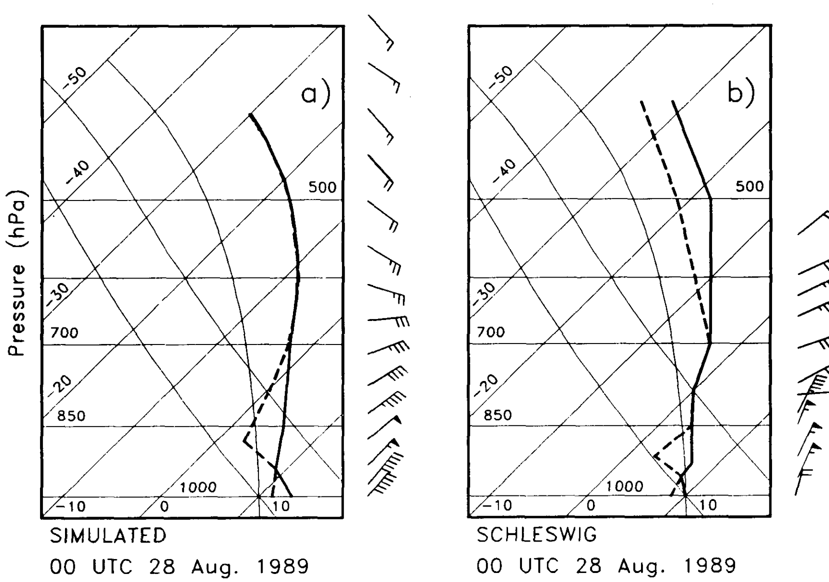

Fig. 6. (a) Sounding for Schleswig, Germany at 00 UTC 28 August 1989, taken from the 24-h model simulation. (b) Actual sounding for Schleswig at 00 UTC 28 August 1989.

A low-level jet in the model is also in good agreement, both in direction and magnitude, with the observed sounding. In the initial wind field (00 UTC 27 August) there is no sign of a low-level jet, so the model has developed this jet in accordance with reality.

Since the model seems to reproduce very well some of the essential features of the weather during the period, we assume that it describes, to a satisfactory degree of accuracy, the main physical processes that took place. Through investigation of the model results, we will therefore in the following section try to answer the question of which physical processes were the main contributors to the interesting weather events that took place during the 24 hours from 00 UTC 27 August.

5. Dynamical processes

5.1. The role of released latent heat

Since the area of heavy precipitation and of sharp pressure gradient coincide, there is reason to believe that a main factor in the development process is the released latent heat. Fig. 7a shows the mean sea level pressure after 24 h model simulation with full physics included, as well as the same quantity for a simulation where the released latent heat is excluded. We see that without latent heat the low over northern Germany has a quite different position, shape and surrounding wind field. This is even clearer in the difference field (Fig. 7b), which constitutes a closed low with a depth of 13 hPa and a horizontal scale of 250 km in the same area where the maximum amount of precipitation occurs. Above the surface, the differences in the height fields are similar up to 850 hPa (maximum 100 geopotential meters), but the maximum difference decreases in strength upward to 72 m at 700 hPa and 10 m at 500 hPa (not shown). Above 500 hPa the differences change sign, the scale becomes larger and the centre is shifted further east.

We may also interpret the differences as a warm core below 500 hPa with a maximum amplitude of 4 K below 850 hPa decreasing to 0.3 K at 500 hPa (not shown). The wind differences are strongest at 925 hPa where the maximum northerly winds reach more than 25 m s^{-1}.

The track of the maximum surface pressure difference is marked in Fig. 7b. It has a more northerly track than the low itself until 24 h, but more southerly afterwards. The maximum surface pressure difference grows from 1 hPa at 09 UTC to 5 at 15 UTC, 9 at 21 UTC and 13 hPa at 03 UTC; later it decreases gradually.

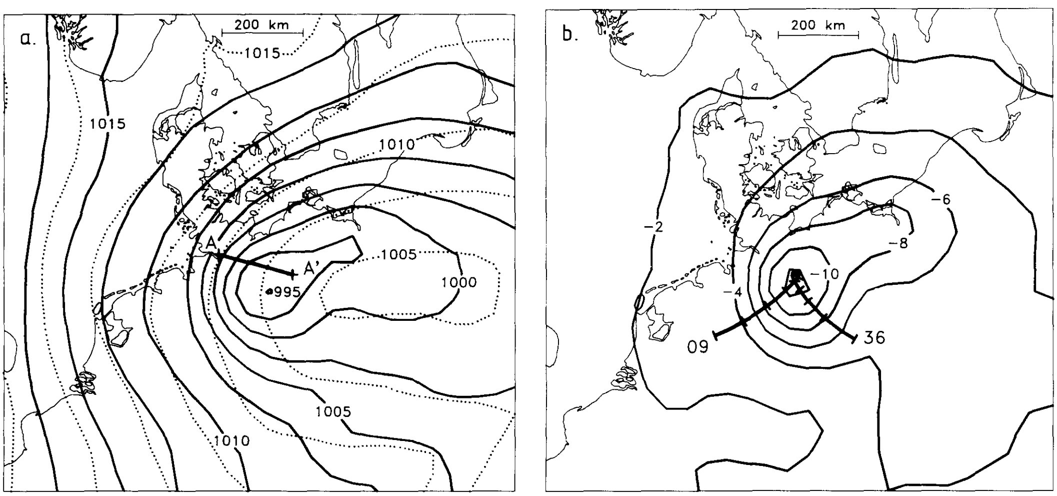

Fig. 7. (a) Solid contours show the regular 24 h simulation of mean sea level pressure (MSLP in hPa), while dotted contours show the 24 h simulation of MSLP (in hPa) in a dry run. Valid at 00 UTC 28 August 1989. (b) Difference in 24 h simulated MSLP (hPa) between the regular and dry runs. The heavy line shows the position of the maximum MSLP difference every 3 h.

The importance of the release of latent heat in forming vigorous storms is well known (e.g., a review paper by Uccellini, 1990). In cases with explosive cyclogenesis the contribution of latent heat to the total deepening of such cyclones has been calculated, for instance, for the October Storm 1987 (Shutts 1990) one third of the deepening was caused by diabatic processes, with release of latent heat as the main factor. The present case shows no explosive cyclogenesis, it is a moderate summer low with a minimum MSLP of 994 hPa and the maximum pressure tendencies are -3 and $+5$ hPa in three hours, respectively (see Table 1). However, during a period of 12 h, a separate mesoscale, warm core low forms in the lower part of the troposphere at the cold side of a cyclone. When released latent heat is excluded, the mesoscale low is completely missing, so that all the deepening of the mesoscale low is caused by the released heat. The resultant of the mesoscale low and main low appears as a strengthening of the pressure gradient west of the main low, and this strengthening seems to be strong enough to change the track of the low to get a component toward the north. Why the track turned again is explained in the next section.

5.2. *Potential vorticity considerations*

From HMR, we know that cyclogenesis can often be explained as a mutual cooperation between a positive anomaly of stratospheric PV being folded downward to mid- or low-level tropospheric heights, a positive temperature anomaly at the surface and a spatial generation of *PV* due to diabatic sources like release of latent heat and friction. It is shown theoretically (Haynes and McIntyre, 1987) that *PV* is spatially redistributed due to diabatic sources confined within the boundaries of a prescribed *PV* domain, not generated or dissipated. In the following we at times still prefer to speak of generation and dissipation of *PV* due to diabatic warming. Release of latent heat is the only significant generating agent on our time scale and the effect of this can be understood from the following equation expressing the material rate of change of *PV* by heat sources:

$$\frac{\mathrm{D}(PV)}{\mathrm{D}t} = \frac{1}{\varrho} \vec{\zeta}_{\mathrm{a}} \cdot \nabla \dot{\theta}.$$

Here, the vorticity vector and the del-operator are three-dimensional, $\dot{\theta} = \mathrm{D}\theta/\mathrm{D}t$ represents the diabatic warming.

On our scale, the horizontal component of vorticity is negligible compared to the vertical component. We see then from the equation that *PV* anomalies are created where the vertical gradient of the heating has its largest values. Below the maximum of released latent heat a positive *PV* anomaly is produced, and above, a negative anomaly (see Fig. 8). The larger the gradient of heating, the larger the anomalies. It is apparent that in order to create a low-level vortex of some intensity, the release of latent heat must take place in a shallow layer (e.g., Bratseth, 1985).

Low-level *PV* caused by release of latent heat starts to grow a few hours into the integration. At 6 h, a maximum of more than 1 PVU is found in a small lump and after 24 h, a maximum of 4 PVU is reached (see Table 2). The rates of production of *PV* is about three times larger than in the case investigated by Davis and Emanuel (1991), and the horizontal scale is much smaller. The height of the maximum is between 850 hPa and 910 hPa all the time. Fig. 9 shows a 3D presentation of the low-level 2.0 PVU surface and the horizontal distribution of *PV* at 9 km at 24 h. The concentrated

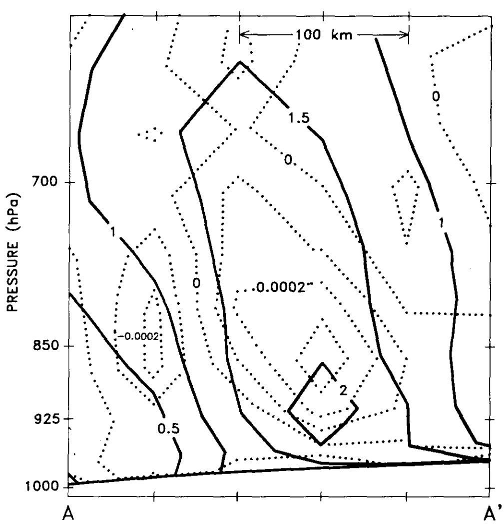

Fig. 8. Cross section along line AA′ in Fig. 7a, showing potential vorticity (solid lines, equidistance 0.5 PVU, 1 PVU equals $10^{-6}\,\mathrm{m^2\,s^{-1}\,K\,kg^{-1}}$), and the latent heating rate (dotted line, equidistance 0.0001 K/s). The cross section is taken after 18 h of integration, i.e., valid at 18 UTC 27 August 1989.

Table 2. *Max low level IPV, pressure level of max low level IPV, and max surface relative vorticity. The unit of IPV is 1 PVU = $10^{-6}\ m^2\ s^{-1}\ K\ kg^{-1}$*

Prog. time (h)	0	3	6	9	12	15	18	21	24	27	30
Max. low level IPV	0.5	0.5	0.8	1.0	1.6	2.0	2.5	3.2	4.2	4.0	3.2
Pressure of max low level IPV (hPa)					850	880	910	900	900	900	850
Max ζ_s ($10^{-4}\ s^{-1}$)	0.5	0.5	1.2	1.8	3.2	3.8	4.7	4.8	5.1	5.0	4.5

low-level mesoscale anomaly is clearly shown, extending from surface to 750 hPa as a near circular configuration with a marked decrease in radius from 850 hPa and upward. Aloft there is a marked *PV* anomaly on a larger scale east of the north-westerly jet over Britain. This anomaly is about to lose contact with its stratospheric reservoir further north.

At this time (24 h), there might be some influence of the upper *PV* anomaly on the structures below. However, earlier on the upper positive anomaly is too far away toward the west to have any influence. In addition, it can be seen from Figs. 12a, c that this anomaly is confined to layers down to the tropopause, which has a minimum height of 7.5 km after 24 h. There is thus nearly no influence of a stratospheric *PV* anomaly in strengthening the low-level low. The spinning up of the low must be explained by the low-level positive anomaly formed by the latent heat release in interaction, as shown by HMR, with the warm surface temperature anomaly (see Fig. 10b). In other words, application of "the invertibility principle" (HMR) on the low-level *PV* anomaly and the surface temperature anomaly will give the wind and temperature structure of the mesoscale disturbance.

Above (below) the level of maximum released latent heat, the static stability decreases (increases). A positive (negative) *PV* anomaly will then develop below (above) the level of maximum released heat. Due to convergence below the

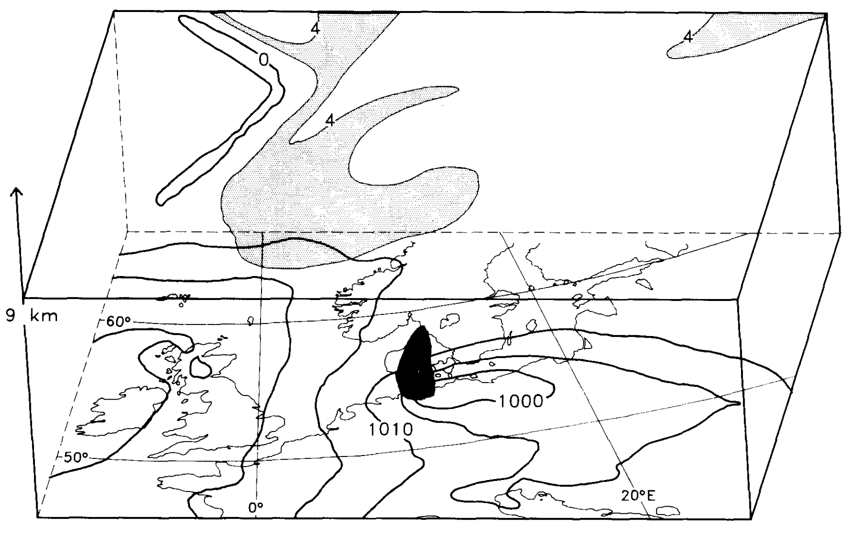

Fig. 9. A 3-dimensional representation of isentropic potential vorticity after 24-h simulation, valid at 00 UTC 28 August 1989. The surface for 2 PVU (1 PVU as in Fig. 8) is shown at the lower levels. The closed surface lies between 750 hPa and 950 hPa. The mean sea level pressure is shown at the surface (5 hPa contours). The upper panel shows horizontal PV distribution at 9000 m. Contour lines are 0 and 4 PVU. Hatched area: PV greater than 4 PVU.

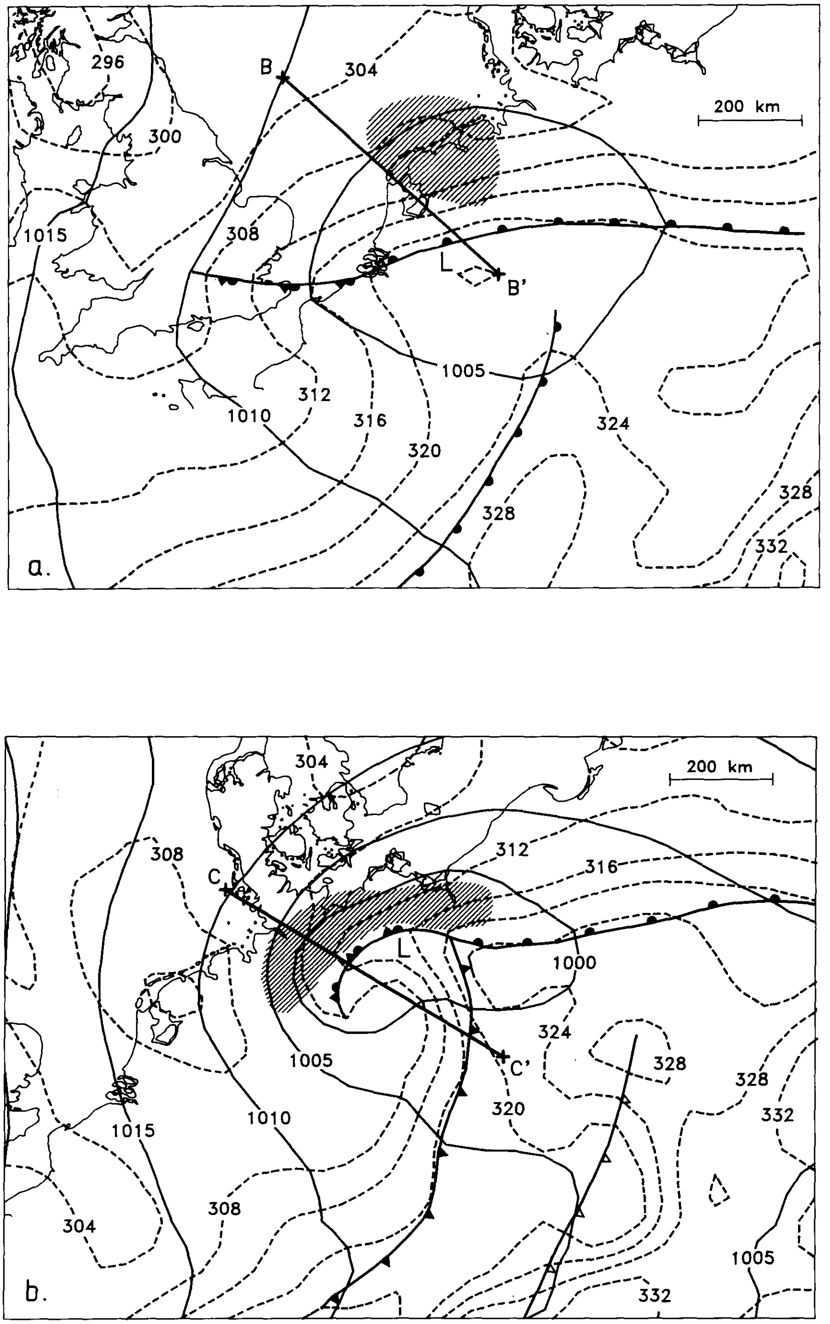

Fig. 10. (a) 6-h simulated MSLP (solid) and θ_e in 925 hPa surface (dashed), valid at 06 UTC 27 August 1989. Hatched area is the area of maximum precipitation (more than 2 mm in 3 h). (b) 24 h simulated MSLP (solid) and θ_e in 925 hPa surface (dashed), valid at 00 UTC 28 August 1989. Hatched area is the area of maximum precipitation (more than 10 mm in 3 h). The surface fronts are subjectively drawn.

positive PV anomaly, there is ascending motion, and thereby destabilization in the layer of the positive anomaly. Under the assumption of PV conservation, the relative vorticity then increases. We might say that some of the "static stability part" of the PV is converted to the "vorticity part". This is clearly seen from Table 2, which shows that the PV increase due to latent heat release is immediately followed by an increase in relative vorticity.

The low-level PV anomaly is formed in an area with marked temperature gradients at the surface (see Fig. 10a and discussion of fronts later on). The wind field surrounding this PV anomaly forms a small scale temperature wave at the surface, in a similar way as in the conceptual model by HMR for explosive cyclones. In the beginning, as the surface temperature wave is growing, the PV anomaly is, as expected, clearly west of the surface wave. After 24 h, the PV anomaly is in phase with the surface warm anomaly, indicating a mature stage, and in agreement with the maximum strength of the low found at this time. The wind field set up by the temperature anomaly cannot strengthen the PV anomaly, since it already has a circular shape in surroundings with small PV values.

The release of latent heat clearly redistributes the upper air PV and builds a negative anomaly above the heat source. At the same time the positive upper anomaly is approaching from the west. The sum of these two anomalies results in a short amplifying wave (see Fig. 9). Eventually this wave seems to supply some divergence to the low-level disturbance and steer its track. After 24-h integration, the maximum divergence above the mesoscale disturbance (more than $10^{-4}\,s^{-1}$) is found between the ridge and the trough of the upper wave, a position where maximum divergence is normally found. However, earlier on maximum upper air divergence is found at the ridge of the amplifying upper wave, at a position where divergence is normally small. This also shows that the cause of the development is the release of latent heat. Any influence of the upper wave at a later stage is a consequence of this development.

The upper wave still amplifies from 24 to 30 h. The positive anomaly penetrates further eastward and gets a position east of the low-level anomaly. The maximum PV of this anomaly is conserved, however, the strength of the anomaly is increased as the negative anomaly is wrapped around on the northern side. The wind field associated with the upper anomaly in this way gets a clear component from the north above the low level PV anomaly which is advected toward the south-east. This explains the turning of the track of the position of the surface low.

5.3. *Fronts and conveyor belts*

A continuation of an occlusion process takes place during the first 24 h of the integration. The position of the fronts, here drawn subjectively on the basis of the horizontal gradients in θ_e, are given in Figs. 10a, b. Since direct transverse circulations are found (see below), most of the gradient is kept on the cold side of the front (e.g., Eliassen, 1990). After 6 h, the temperature wave is clear at the surface (Fig. 10a). The warm front is well defined and extends a little westward from the low centre. The front is elongated further westward in the same direction toward England as an occlusion, much as the subjective analysis (see Fig. 2a). The warm front is steep and continues throughout most of the troposphere (Fig. 11). The gradients across the cold front disappear close to the warm front (Fig. 10a). This is in accordance with the

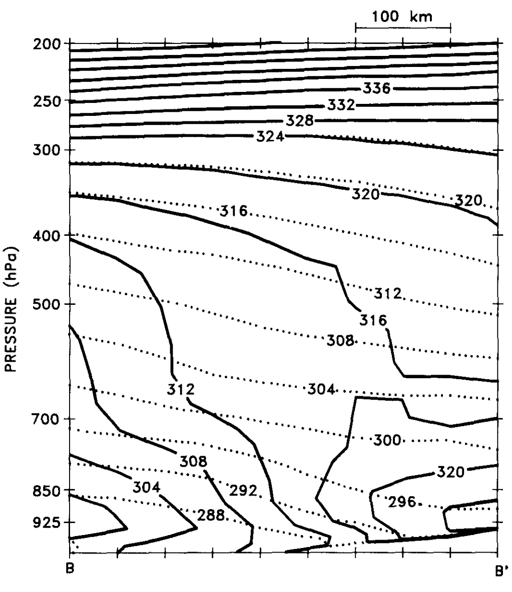

Fig. 11. Cross section along line BB′ in Fig. 10a. Equivalent potential temperature (solid lines) and potential temperature (dotted lines), both with equidistance 4 K.

conceptual front model of Shapiro and Keyser (1990).

After 24 h, the warm front has moved northeastward (Fig. 10b), while the cold front has moved toward the east. The cold front is now indistinct at the surface, however, it is well defined above 850 hPa and the positioning in Fig. 10b is made according to its position aloft.

As mentioned, the created mesoscale *PV* anomaly forms a smaller scale temperature wave on the warm occlusion. In this way a regeneration of the fronts takes place with a normal frontal evolution ending in an occlusion process. Fig. 10b shows the structure after 24 h. A new cold front has developed further west. This front is limited to layers below 700 hPa and is clearly identified from

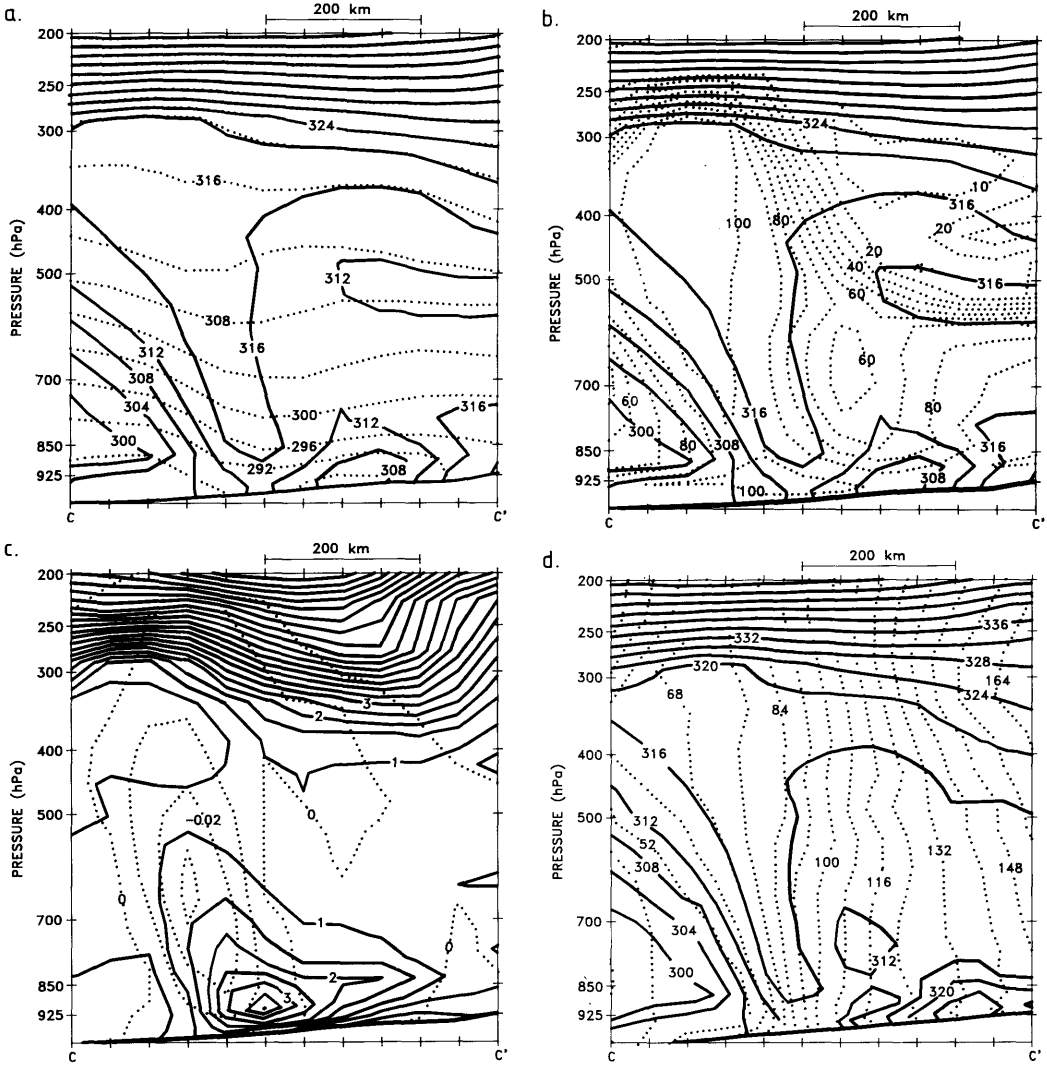

Fig. 12. (a), (b), (c) and (d). Cross section along line CC′ in Fig. 10b after 24 h of integration, valid at 00 UTC 28 August 1989. (a) Same fields as in Fig. 11. (b) Equivalent potential temperature (solid lines, equidistance 4 K) and relative humidity (dotted lines, equidistance 10%). (c) Potential vorticity (solid lines, 1 PVU and equidistance as in Fig. 8) and ω (dp/dt) (dotted lines, unit hPa s^{-1}). (d) Equivalent potential temperature (dotted lines, equidistance 4 K) and angular momentum M (solid lines, equidistance 8 ms^{-1}) ($M = fy - u$, where y is distance along the cross-section and u horizontal wind component normal to the cross-section).

Tellus A/46/5-7

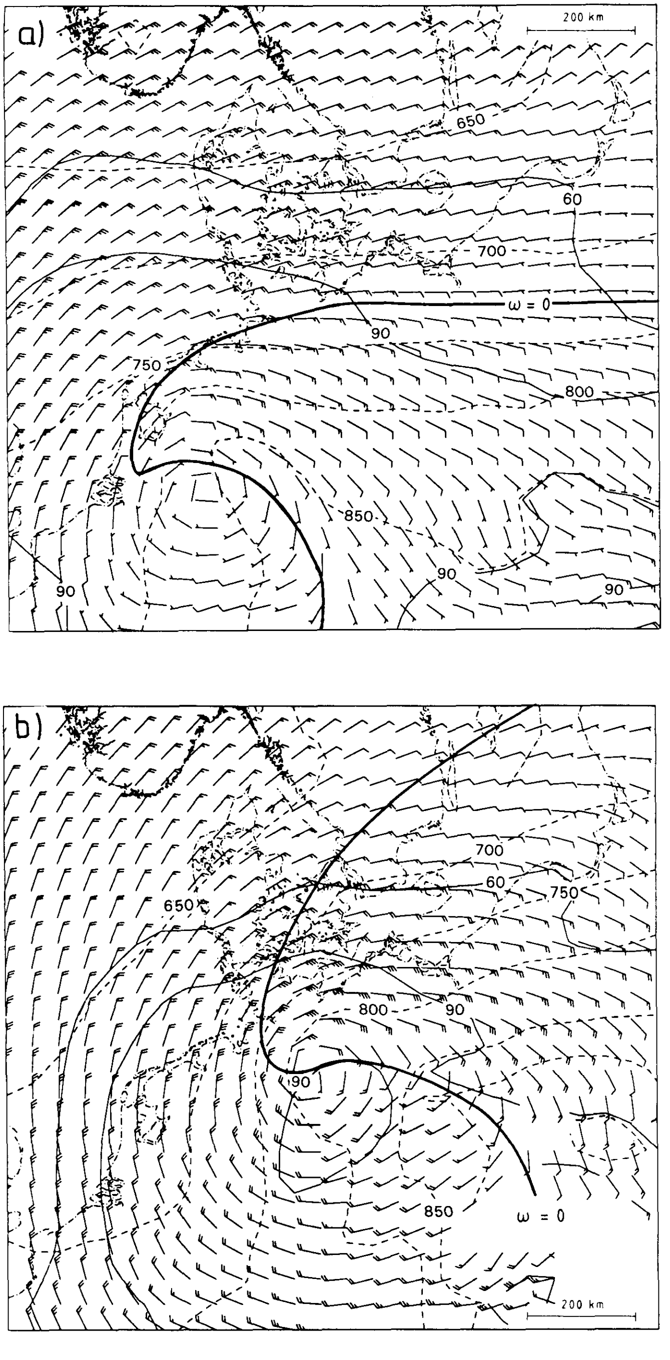

Fig. 13. (a) 6-h simulation of pressure (dashed contours in hPa), horizontal wind relative to the moving low pressure system and relative humidity (only 60% and 90% solid contours) in the 297.5 K isentropic surface. Valid at 06 UTC 27 August 1989. Heavy line: zero vertical velocity (ω). (b) Same as (a) but an 18-h simulation valid at 18 UTC 27 August 1989.

the distribution of θ_e at the surface (Fig. 10b). The cold air west of the front is in a process of secluding a warm core anomaly at the tip of the occlusion. However, a complete seclusion with closed isotherms as in the conceptual model by Shapiro and Keyser (1990) is missing. Contrary to the main cold front this secondary front extends all the way to the occlusion point.

The areas of heavy precipitation are associated with the warm front in the beginning, but later with the occlusion (Figs. 10a, b). If we compare the position of maximum precipitation with the position of maximum potential vorticity produced by release of latent heat, they almost coincide and follow in time (not shown). This indicates that the PV anomaly and the production area of PV nearly overlap. In this way additional generation of PV will increase the existing anomaly.

Cross-sections through the fronts at 06 and 24 hours are given in Figs. 11, 12 respectively. After 6 h, the warm front is well developed (Fig. 11) with a direct vertical circulation with rising warm, moist air in a rather deep layer with small static stability (not shown). After 24 h, a cross-section taken trough the occlusion shows a warm, humid core (high values of θ_e) with a strong, steep front north of the core (Fig. 12a). The secondary circulation with rising warm, humid air and sinking cold, dry air is now stronger (Figs. 12b, c). Conditional symmetric instability has been investigated by looking at the variation of absolute momentum along surfaces of constant θ_e (Fig. 12d). Neutral areas are found at the warm side of the front, and indication of symmetric instability and vertically conditionally unstable air is found on the southern side of the warm core. The shallow cold front is seen on the right end of the cross-section.

The conveyor belts related to the fronts have been studied by computing three-dimensional trajectories and isentropic maps with horizontal wind relative to a coordinate system following the low (Figs. 13a, b). Assuming adiabatic conditions, the vertical velocity is given by relative horizontal wind multiplied with the pressure gradient in the direction of the wind. In Fig. 13 the surface of 297.5 K has been chosen, it intersects the front with warm air at low levels and cold air at higher levels further north. A warm conveyor belt is related to the warm front and the occlusion. It rises toward the north-west with a westward component relative to the front. Normally the warm conveyor belt is connected to a cold front and usually turns to the right as it reaches the warm front, with a main component along this front away from the low centre (Browning, 1990). In our case the warm conveyor belt is strongly convergent toward the tip of the occlusion and provides humidity for heavy precipitation being produced over a relatively small horizontal area. This is seen from the three-dimensional trajectories from initial time to 24 h shown in Fig. 14. Three of the trajectories show the convergent low-level warm conveyor belt, which continues in strong lifting to 8000 m over a small area with divergent trajectories aloft. The trajectory reaching the highest level has a clear origin in the warm air, the two others start in the frontal zone.

As the low is strengthened, convergence increases in the boundary layer. In this way humid surface air from the cold side of the low, mainly from the Baltic and the North Sea, is also being pumped into the low. This is seen from one of the trajectories in Fig. 14. At some distance from the low centre the vertical displacements are small.

5.4. Comparison with the Baltic Case

We have rerun the storm of 23 July 1985 in the Baltic described by Kristjansson (1990). This is

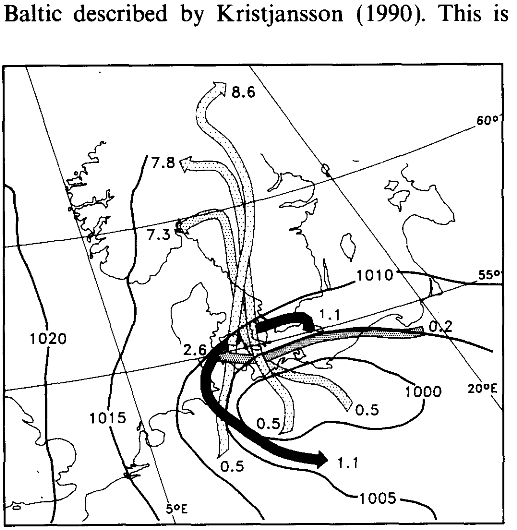

Fig. 14. A 3-dimensional representation of simulated trajectories from initial time 00 UTC 27 August 1989 and 24 h forward. Numbers give the hight in km at the start and the end of the trajectories. The three trajectories with largest vertical displacement all start at 0.5 km. At the surface is placed MSLP (hPa) after 24 h, valid at 00 UTC 28 August 1989. For position of the surface low see Fig. 3.

also a mesoscale summer case with a secondary development caused by release of latent heat in connection with the occlusion of the frontal system. As in our case the surface pressure gradients are strengthened at the cold side of a weak low and the precipitation is heavy over a small area. A similar low-level *PV* anomaly is found (not shown). This mesoscale anomaly is caused by release of latent heat in combination with a low-level temperature wave. Maximum *PV* reaches 4 units in less than 12 h. Also in the Baltic case the warm conveyor belt flows toward the north-west with a westerly component along the occlusion (not shown).

6. Concluding remarks

This case study has been on an unexpected mesoscale reinforcing of a weak summer low taking place over land in Northern Germany on 27 and 28 August 1989. The development occurred on the occlusion and was experienced as a strengthening of the surface pressure gradient in the cold air north of the low, accompanied by large amounts of rain (more than 100 mm in 24 h). It has been shown that the development is caused by release of latent heat organised inside the weak low. The development is a warm core disturbance below 500 hPa with a diameter of 250 km, growing to a surface pressure amplitude of 13 hPa in about 12 h with maximum wind speed of 15 m s^{-1} superimposed on the existing flow. In this respect the development has some similarities to CISK, however, the process starts with lifting of moist warm air on the occlusion and not with convection as assumed in CISK. Bergeron (1954) studied regenerations taking place on the occlusion of extratropical cyclones. He maintained that such developments might take place, as he said "in a tropical hurricane style". The present case might be characterized as such a regeneration, the low develops on the occlusion and the mesoscale structure has a warm core, near circular shape.

The mesoscale development, which occurs over land within a rather weak and innocent-looking low moving into Northern Germany from the North Sea, seems to be generated through release of latent heat alone. This heat forms a low-level near circular organization of *PV*, which within 12 h grows from a maximum value of 1 PVU to 4 PVU. This mesoscale *PV* anomaly forms a temperature wave at the surface. Using the invertibility principle for *PV* (see HMR), this anomaly and the surface temperature anomaly are considered to give the vortex described above. The released heat causes a redistribution of *PV* in the upper troposphere, which together with an approaching *PV* anomaly from the west results in an amplifying short wave, which eventually steers the track of the low and probably supports the mesoscale disturbance with divergence at its top.

It is well-known that release of latent heat plays an important role in nearly all extensive cyclogenesis. Normally the main heat release takes place on the eastern side of a low as it moves eastward. The potential vorticity distribution will typically deform along the fronts and might be advected away from its source. In this way the effect of the heat release will be spread around the cyclone and strengthening of troughs is the usual response. In the present case it is different, further release of latent heat takes place in such a way that the existing *PV* anomaly is strengthened. The near circular shaped low-level *PV* anomaly is the most important signature of the development.

The evolution might be divided in two stages. The synoptic scale low representing the first stage provides the necessary finite amplitude, with some low-level convergence, for the CISK-like second stage to be started. In this way the development is in accord with the discussion on CISK by van Delden (1989), who stresses that a finite starting amplitude must be present before the instability might start. A warm, humid conveyor belt from the south and south-east converges at low levels and rises over a relatively small area, providing abundance of humidity to the disturbance.

It is considered that CISK plays an important part in strong polar lows (e.g., Økland, 1977; Rasmussen, 1977, 1979), and in this respect the dynamical development in the present case bears some similarities to that of polar lows in the Norwegian Sea. However, it is believed that all polar lows are connected or initiated by disturbances aloft (Økland, 1989; Nordeng and Rasmussen, 1992). This is different from our case where high level influences are weak in the beginning.

The mesoscale development has been compared with the so-called "Baltic Storm" (Kristjansson, 1990), which took place close to the island Øland (about 57° North and 17° East) 23 July 1985.

Except that the Baltic case developed over sea, clear similarities between the two cyclogeneses are found. In both cases regeneration took place on the occlusion of a weak low travelling eastward. Unexpectedly strong northerly winds and large amounts of precipitation were found in the rear of both lows, and a large anomaly of low-level *PV* beneath the areas where latent heat was released. The time scale for the growth of the anomaly was 12 hour in both cases.

Both in the present case and in the Baltic Storm the operational version of the numerical model failed to develop the correct intensity of the meso-scale disturbance. Precipitation rates were smaller and the released heat was distributed in a deeper layer (Kristjansson, 1990). In the Sundqvist scheme convection may start only from particles in the boundary layer, while in the NOLAM model possible convection is checked at every model layer. We believe this difference might be one reason for the stronger vertical concentration of the heat and the stronger development found with the Sundqvist scheme.

7. Acknowledgements

The authors want to express their gratitude to Mr. F. Cleveland who prepared the figures. The work was partially supported by a grant from The Norwegian Research Council for Science and Humanities (NAVF).

REFERENCES

Bergeron, T. 1954. Reviews of tropical hurricanes. *Quart. J. Roy. Meteor. Soc.* **80**, 131–164.

Blackadar, A. K. 1979. High resolution models of the planetary boundary layer. *Advances in Environment and Scientific Engineering*. London: Gordon and Breach. 276 pp.

Bratseth, A. M. 1982. A simple and efficient approach to the initialization of weather prediction models. *Tellus* **34**, 352–357.

Bratseth, A. M. 1983. Some economical, explicit finite-difference schemes for the primitive equations. *Mon. Wea. Rev.* **111**, 663–668.

Bratseth, A. M. 1985. A note on CISK in polar air masses. *Tellus* **37A**, 403–406.

Bratseth, A. M. 1987. *Efficient dynamical initialization of a limited area model.* Rep. No. 65, Institute of Geophysics, University of Oslo, Norway.

Bratseth, A. M. 1989. Efficient dynamical initialization of a limited area model. *Tellus* **41A**, 18–31.

Browning, K. A. 1990. Organization of clouds and precipitation in extratropical cyclones. *The Eric Palmén Memorial Volume*. Amer. Meteor. Soc., Boston, USA, 129–154.

Brown, H. A. and Campana, K. A. 1978. An economical time-differencing system for numerical weather prediction. *Mon. Wea. Rev.* **106**, 1025–1036.

Davis, C. A. and Emanuel, K. A. 1991. Potential Vorticity Diagnostics of Cyclogenisis. *Mon. Wea. Rev.* **119**, 1929–1953.

Eliassen, A. 1956. *A procedure for numerical integration of the primitive equations of the two-parameter model of the atmosphere*. Sci. Rept. no. 4, Dept. of Meteorology, UCLA.

Eliassen, A. 1990. Transverse Circulations in Frontal Zones. *The Eric Palmén Memorial Volume*. Amer. Met. Soc., Boston, USA, 155–166.

Geleyn, J.-F. 1985. On a simple parameter-free partition between moistening and precipitation in the Kuo scheme. *Mon. Wea. Rev.* **113**, 406–407.

Grønås, S. 1990. Early results with the new Norwegian high resolution operational NWP models. *Hirlam Workshop on Mesoscale modelling*. HIRLAM Technical Report No. 8.

Grønås, S. and Hellevik, O. E. 1982. *A limited area prediction model at the Norwegian Meteorological Institute*. Techn. Rep. no. 61, The Norwegian Meteorological Institute, Oslo, Norway.

Grønås, S. and Midtbø, K. H. 1987. Operational multivariate analyses by successive corrections. Short- and medium-range numerical weather prediction. *J. Meteor. Soc. Japan* (Tokyo, Japan), Special Volume.

Grønås, S., Foss, A. and Lystad, M. 1987. Numerical simulations on polar lows in the Norwegian Sea. *Tellus* **39A**, 334–353.

Haynes, P. H. and McIntyre, M. E. 1987. On the evolution of vorticity and potential vorticity in the presence of diabatic heating and frictional and other forces. *J. Atmos. Sci.* **44**, 828–841.

Hoskins, B. J., McIntyre, M. E. and Robertson, A. W. 1985. On the use and significance of isentropic potential vorticity maps. *Quart. J. Roy. Meteor. Soc.* **111**, 877–946.

Kristjansson, J. E. 1990. Model simulations of an intense meso-beta scale cyclone. The role of condensation parameterization. *Tellus* **42A**, 78–91.

Kvamstø, N. G. 1992. *Implementing the "Sundqvist scheme" in the Norwegian Limited Area model.* Meteorological Report Series, University of Bergen 2-1992. Dept. of Geophysics, Univ. of Bergen, Allégaten 70, N-5007 Bergen, Norway.

Kuo, H. L. 1965. On formation and intensification of Tropical Cyclones through latent heat release by cumulus convection. *J. Atmos. Sci.* **22**, 40–63.

Kuo, H. L. 1974. Further studies of parameterization of the influence of cumulus convection on large-scale flow. *J. Atmos. Sci.* **31**, 1232–1240.

Louis, J.-F., Tiedtke, M. and Geleyn, J.-F. 1981. A short history of the PBL-parameterization at ECMWF. *Proceedings of the Workshop on Planetary boundary layer parameterization.* European Centre for Medium range Weather Forecasts. Shinfield Park, Reading, England.

Manabe, S., Smagorinsky, J. and Strickler, R. F. 1965. Simulated climatology of a general circulation model with a hydrological cycle. *Mon. Wea. Rev.* **89**, 503–532.

Nordeng, T. E. 1986. *Parameterization of physical processes in a 3-dimensional numerical weather prediction model.* Technical Report No. 65. The Norwegian Meteorological Institue, Oslo, Norway.

Nordeng, T. E. and Rasmussen, E. A. 1992. A most beautiful polar low. A case study of a polar low development in the Bear Island region. *Tellus* **44A**, 81–99.

Økland, H. 1977. *On the intensification of small-scale cyclones formed in very cold air masses heated over the ocean.* Inst. Rep. Ser. No. 26, Dept of Geophyics, Univ. of Oslo, Norway, 25 pp.

Økland, H. 1989. On the genesis of polar lows. In: *Polar and arctic lows* (eds. P. F. Twitchell, E. A. Rassmussen and K. L. Davidson). A Deepak Publishing, Hampton, Vi., USA, 179–190.

Rasmussen, E. A. 1977. *The Polar Low as a CISK Phenomenon.* Rep. No. 6, Inst. Theoret. Meteor., Univ. of Copenhagen, Copenhagen, 77 pp.

Rasmussen, E. A. 1979. The polar low as an extratropical CISK disturbance. *Quart. J. Roy. Meteor. Soc.* **105**, 531–549.

Shapiro, M. A. and Keyser, D. 1990. Fronts, jet streams and the tropopause. The *Eric Palmén Memorial Volume.* Amer. Meteor. Soc., Boston, USA, 167–193.

Shutts, G. J. 1990. Dynamical aspects of the October storm, 1987: A study of a successful simulation. *Quart. J. Roy. Meteor. Soc.* **116**, 1315–1347.

Sundqvist, H., Berge, E. and Kristjansson, J. E. 1989. Condensation and cloud parameterization studies with a mesoscale NWP model. *Mon. Wea. Rev.* **117**, 1641–1657.

Uccellini, L. W. 1990. Processes contributing to the rapid development of extratropical cyclones. Extratropical Cyclones. *The Erik Palmén memorial volume.* Amer. Meteor. Soc., Boston, USA, 81–106.

Van Delden, A. 1989. Gradient wind adjustment, CISK and the growth of polar lows by diabatic heating. In: *Polar and arctic lows* (eds. P. F. Twitchell, E. A. Rasmussen and K. L. Davidson). A Deepak Publishing, Hampton, Vi., USA, 109–130.